NeuroImage: Clinical 49 (2026) 103947

Contents lists available at ScienceDirect

NeuroImage: Clinical

journal homepage: www.elsevier.com/locate/ynicl

Resting-State EEG captures functional network correlates of plasma p-Tau-217 in Alzheimer's disease

Giordano Cecchetti [a,b,c,1,2], Jacopo Lanzone [b,f,1,3], Luca Zanchi [c,f,4], Giulia Rugarli [a,c,d,5], Silvia Basaia [c,f,6], Marco Cursi [b,7], Federico Coraglia [a,d,8], Edoardo G. Spinelli [a,c,d,9], Alma Ghirelli [a,c,d,10], Elisa Canu [a,c,f,11], Elisa Sibilla [a,c,d], Francesca Caso [a,12], Roberto Santangelo [a,b,13], Davide Curti [b], Giovanna Franca Fanelli [b], Anna Bellini [b], Giuseppe Magnani [a,14], Federica Agosta [a,c,d,f,15], Massimo Filippi [a,b,c,d,e,f,16,*]

[a] Center for Alzheimer's Disease and Related Disorders (CARD), Neurology Unit, IRCCS San Raffaele Scientific Institute, Milan, Italy
[b] Neurophysiology Service, IRCCS San Raffaele Scientific Institute, Milan, Italy
[c] Neuroimaging Research Unit, Division of Neuroscience, IRCCS San Raffaele Scientific Institute, Milan, Italy
[d] Vita-Salute San Raffaele University, Milan, Italy
[e] Neurorehabilitation Unit, IRCCS San Raffaele Scientific Institute, Milan, Italy
[f] Neurotech Hub, Vita-Salute San Raffaele University, Milan, Italy

ARTICLE INFO

Keywords:
Alzheimer's disease
EEG
P-tau217
Plasma biomarkers

ABSTRACT

Background: Scalable biomarkers are needed for early Alzheimer's disease (AD) detection. Plasma p-tau217 reflects AD pathology, while resting-state EEG captures functional brain alterations. Their relationship remains unclear.

Methods: We enrolled 128 patients with subjective cognitive decline (SCD), mild cognitive impairment due to AD (AD-MCI), or AD dementia (AD-DEM), who underwent 32-channel EEG and plasma biomarker assessment. EEG

Abbreviations: AD, Alzheimer's disease; AD-DEM, mild dementia due to Alzheimer's disease; AD-MCI, mild cognitive impairment due to Alzheimer's disease; AUC, area under the curve; EEG, electroencephalography; MSE, multiscale entropy; PAC, phase–amplitude coupling; p-tau217, plasma phosphorylated tau at threonine 217; ROC, receiver operating characteristic; SCD, subjective cognitive decline.

* Corresponding author.
E-mail addresses: cecchetti.giordano@hsr.it (G. Cecchetti), lanzone.jacopo@hsr.it (J. Lanzone), zanchi.luca@hsr.it (L. Zanchi), rugarli.giulia@hsr.it (G. Rugarli), basaia.silvia@hsr.it (S. Basaia), cursi.marco@hsr.it (M. Cursi), coraglia.federico@hsr.it (F. Coraglia), spinelli.edoardogioele@hsr.it (E.G. Spinelli), ghirelli.alma@hsr.it (A. Ghirelli), canu.elisa@hsr.it (E. Canu), sibilla.elisa@hsr.it (E. Sibilla), caso.francesca@hsr.it (F. Caso), santangelo.roberto@hsr.it (R. Santangelo), magnani.giuseppe@hsr.it (G. Magnani), agosta.federica@hsr.it (F. Agosta), filippi.massimo@hsr.it (M. Filippi).
[1] These authors contributed equally to this work.
[2] https://orcid.org/0000-0002-6544-410X.
[3] https://orcid.org/0000-0001-7217-6281.
[4] https://orcid.org/0009-0002-2734-5749.
[5] https://orcid.org/0009-0004-2063-7735.
[6] https://orcid.org/0000-0002-0722-6243.
[7] https://orcid.org/0000-0002-7928-0417.
[8] https://orcid.org/0009-0008-7717-6406.
[9] https://orcid.org/0000-0003-1492-7221.
[10] https://orcid.org/0000-0001-8440-1036.
[11] https://orcid.org/0000-0001-5804-3378.
[12] https://orcid.org/0000-0002-3072-1218.
[13] https://orcid.org/0000-0002-8760-2703.
[14] https://orcid.org/0000-0001-8436-2903.
[15] https://orcid.org/0000-0003-3121-4979.
[16] https://orcid.org/0000-0002-5485-0479.

https://doi.org/10.1016/j.nicl.2026.103947
Received 29 September 2025; Received in revised form 7 January 2026; Accepted 8 January 2026
Available online 10 January 2026

Machine learning
Network dysfunction

features included spectral, aperiodic, phase–amplitude coupling, and complexity metrics. Machine learning was used to classify p-tau217 positivity.
Results: AD-MCI and AD-DEM patients showed increased p-tau217 and spectral slowing (higher theta, lower alpha). While no correlations survived correction for multiple comparisons, stage-specific analyses revealed positive associations between theta power and p-tau217 in AD-MCI and AD-DEM. A random forest classifier achieved an AUC of 0.75 in predicting p-tau217 positivity.
Conclusions: EEG captures functional alterations reflecting AD pathology beyond molecular measures, supporting its value as a complementary, non-invasive biomarker for early stratification in clinical settings.

1. Background

Alzheimer's disease (AD) is the most prevalent cause of dementia worldwide and a growing public health challenge, with an expected tripling of cases by 2050. (Scheltens et al., 2021) The pathophysiological processes of AD (amyloid-β deposition and tau pathology) begin decades before clinical symptoms, underscoring the urgency of early diagnosis and accurate biological stratification. (Jack et al., 2018) Cerebrospinal fluid (CSF) and amyloid PET (positron emission tomography) imaging are reliable in identifying AD pathology; however, their invasiveness, high cost, and limited accessibility restrict their use primarily to tertiary care centers. These modalities are often impractical in community or primary care settings, contributing to a substantial gap in diagnostic access and care between patients followed at specialized memory clinics and those managed in routine clinical practice. This has prompted growing interest in minimally invasive, scalable biomarkers that could support early diagnosis across the broader healthcare system. Among these, plasma phosphorylated tau at threonine-217 (p-tau217) has emerged as a particularly promising biomarker. (Jack et al., 2024) Several studies have shown that p-tau217 not only correlates with amyloid and tau PET burden but also differentiates AD from other neurodegenerative disorders, including at early stages such as mild cognitive impairment (MCI) and even subjective cognitive decline (SCD). (Palmqvist et al., 2020; Janelidze et al., 2021; Cecchetti et al., 2024).

Complementing molecular biomarkers, electroencephalography (EEG) offers a non-invasive, cost-effective, and scalable method to assess functional brain alterations associated with AD. Quantitative EEG markers such as spectral slowing (increased theta, reduced alpha), lower individual alpha frequency, decreased signal complexity, and flattening of the 1/f spectral slope have all been consistently associated with AD pathology. (Dauwels et al., 2011; Smailovic et al., 2018; Cecchetti et al., 2021; Cecchetti et al., 2024; Cecchetti et al., 2024; Chetty et al., 2024) Prior studies from our group and others have demonstrated that these changes are detectable not only in established dementia but also in MCI and SCD, and that they correlate with CSF and imaging biomarkers of amyloid and tau pathology. Notably, resting-state EEG has revealed early signs of network dysfunction and disconnection, which may precede structural atrophy and cognitive decline.

These findings indicate that while both EEG and plasma biomarkers can detect AD pathology, they capture distinct and complementary aspects of the neurodegenerative cascade: p-tau217 reflects molecular pathology, whereas EEG captures its functional impact on brain networks. We posit that the joint use of these non-invasive markers could improve detection of early cases and in general patients' risk stratification.

To the best of our knowledge, no studies have investigated the relationship between EEG features and AD plasma biomarkers, particularly in real-world clinical populations. In this study, we address this gap by exploiting a well-characterized cohort from a tertiary memory clinic to: (1) compare plasma biomarker levels and EEG features across patients with SCD, MCI due to AD (AD-MCI), and mild AD dementia (AD-DEM); (2) examine whether EEG signatures reflect plasma-defined AD pathology through correlation and stage-specific analyses; and (3) evaluate whether EEG-based machine learning models can predict p-tau217 positivity.

2. Methods

2.1. Participants

This cross-sectional study included consecutive individuals referred to the Center for Alzheimer's disease and related disorders (CARD), Neurology Unit, IRCCS San Raffaele Scientific Institute (Milan, Italy), between October 2023 and December 2024, for the evaluation of cognitive complaints.

Inclusion criteria for the patient group were: (i) a clinical diagnosis of SCD, AD-MCI (corresponding to stage 3 of the 2024 NIA-AA classification), or AD-DEM (stage 4);(3) (ii) availability of venous blood sampling for plasma biomarker analysis (p-tau217, p-tau181, Aβ42, Aβ40); and (iii) availability of a 32-channel resting-state EEG.

Diagnoses were made by an experienced neurologist following a comprehensive diagnostic work-up, which included neuropsychological testing, structural neuroimaging (MRI or CT), plasma biomarkers, and, when clinically indicated, CSF analysis or amyloid PET imaging. Apolipoprotein E genotyping was also performed in a subset of patients.

The 32-channel resting-state EEG was obtained within three months following venous blood sampling for plasma biomarker analysis.

A group of cognitively unimpaired healthy controls (HC) was also included for the EEG analyses. HC participants were recruited among volunteers, caregivers, and non-consanguineous relatives of patients. They were required to have a normal neuropsychological profile and no history of neurological or major psychiatric disorders. HC were not included in the plasma biomarkers analyses due to ethical considerations related to the management of potential incidental pathological findings.

Exclusion criteria for all participants included: a history of major psychiatric disorders (e.g., major depressive episode); current or past substance abuse with potential impact on cognition or cortical electrical activity; evidence of focal or diffuse brain damage on neuroimaging, clinical signs or symptoms suggestive of non-Alzheimer's neurodegenerative conditions (e.g., frontotemporal dementia, Lewy body dementia); and a personal history of epilepsy.

All participants provided written informed consent prior to inclusion. The study was approved by the Ethics Committee of IRCCS San Raffaele Scientific Institute and conducted in accordance with the Declaration of Helsinki and its subsequent amendments. Samples collected for research purposes were processed and stored at the institutional biobank, Biological Resource Center (CRB-OSR) (Num ID CRB in BBMRI-ERIC: bbmri-eric:ID:IT_1383758011993577).

2.2. Plasma collection and biomarkers measurement

Blood withdrawal for plasma collection was performed in dipotassium EDTA anticoagulant tubes through venipuncture for all patient groups. Blood samples were centrifuged for 10 min at 2000 g; plasma was then aliquoted in 1 mL portions into polypropylene tubes and stored at − 80 °C until analysis. Prior to measurement, samples were thawed at room temperature for 30 min, vortexed for 10 s, and centrifuged again for 5 min at 2000 g. Levels of plasma Aβ42, Aβ40, p-tau181, and p-tau217 were measured using fully automated chemiluminescent enzyme immunoassay (CLEIA) on the LUMIPULSE G600II system (Fujirebio),

following manufacturer instructions, as previously described (6).

2.3. EEG recording and preprocessing

Resting-state EEG was recorded using a 32-channel Micromed BRAIN QUICK® system (SystemPlus software; Micromed, Mogliano Veneto, IT) with a standard 10–20 electrode montage. (Nuwer et al., 1998) Ten minutes of eyes-closed EEG were acquired in a quiet, dimly lit room to minimize eye movement and muscle artifacts. The awake state was continuously monitored via real-time visual inspection to exclude drowsiness or sleep. EEG signals were sampled at 256 Hz with 16-bit A/D conversion and referenced to electrode AFz. Electrode impedance was kept below 5 kΩ. EEG data were exported in EDF format for offline analysis.

Eyes-closed resting-state segments were retained for analysis. Preprocessing was carried out using EEGLAB (v2024.2.0; Delorme & Makeig, 2004) and custom MATLAB scripts (R2023b; MathWorks). The preprocessing pipeline included the following steps: detrending; high-pass filtering above 1 Hz; average referencing; Artifact Subspace Reconstruction (ASR, EEGlab clean_rawdata, including a burst criterion of 20 standard deviations for high-amplitude artifact detection); (Chang et al., 2020) bad channels interpolation; low-pass filtering below 70 Hz; and notch filtering at 50 Hz. Filtering was performed using a zero-phase finite impulse response (FIR) filter implemented in EEGLAB (pop_eegfiltnew). Filter order was automatically determined based on the transition bandwidth relative to the sampling rate, following EEGLAB default heuristics. Independent component analysis (ICA) was then applied, and ICLabel was used to automatically identify and reject non-neural components such as eye movements, muscle artifacts, and other noise sources. (Pion-Tonachini et al., 2019) ICA was performed using the runICA algorithm, and on average 4.41 ± 1.93 independent components per subject were rejected. Each rejection step was automatically back-tested to verify that it preserved an adequate amount of signal variability (i.e., post-cleaning signal variance $\geq$ 95 % of pre-cleaning variance), triggering an alert if this threshold was exceeded. Preprocessing was supervised to avoid rejection of brain components, verify the quality and determine whether further correction was necessary. An automated summary report was generated for each EEG. This included a butterfly plot, power spectral density (PSD), topographic maps for canonical frequency bands (delta, theta, alpha, beta, and low gamma), time–frequency representations, and ICA component classifications. An experienced EEG specialist reviewed these outputs to confirm data quality and determine final inclusion.

2.4. EEG feature extraction

EEG feature extraction was performed using MNE-Python and custom Python code. (Eric, 2024) From each preprocessed EEG, we selected a 180-second artifact-free segment of eyes-closed resting-state activity. Clean segments were defined as those requiring minimal corrective interventions, such as segment removal or signal reconstruction via ASR.

Two main categories of features were extracted: frequency-domain and complexity-based metrics.

For the frequency-domain analysis, relative power values were computed for standard EEG frequency bands (delta, theta, alpha, beta, low gamma). Electrodes were grouped into predefined scalp regions of interest (ROIs) – Frontal, Temporal, Parietal, Occipital, and Somatosensory – separately for the left and right hemispheres. Band-specific relative power was calculated within each ROI, and asymmetry indices (left/right) were derived for each frequency band. In addition, spectral parameters were derived using the FOOOF (Fitting Oscillations and One-Over-F) algorithm, (Donoghue et al., 2020) including the exponent and offset of the 1/f aperiodic background, as well as the frequency and amplitude of the spectrum peak. FOOOF was applied to power spectra computed in the 1–70 Hz range, using a peak width range of 1–6 Hz, a minimum peak height of 0.15, and a maximum of four peaks. We also assessed phase–amplitude coupling (PAC), quantifying how the phase of low-frequency oscillations modulates the amplitude of higher-frequency activity, as previously demonstrated in human neocortex. (Canolty et al., 2006) Specifically, we focused on theta–low gamma coupling, using the pactools Python package and custom code. (Dupre la Tour et al., 2017).

For the complexity-related domain, we computed three nonlinear metrics: Higuchi's fractal dimension, multiscale entropy, and the Lempel-Ziv complexity coefficient, using the NeuroKit2 toolbox. (Makowski et al., 2021) For multiscale entropy, the optimal embedding dimension was first estimated for each EEG signal using the complexity_dimension function (delay = 1, maximum dimension = 20), applying the average false nearest neighbors (AFN) method. The embedding dimension returned by this procedure was then used as input for the multiscale entropy computation, which was performed across default scale factors. Lempel–Ziv complexity was computed on normalized signals (normalize = True), while Higuchi's fractal dimension was estimated on 2-second epochs using the default maximum k parameter implemented in NeuroKit2. These measures were used to capture the signal's temporal irregularity and richness across multiple time scales.

In total, 51 EEG features were extracted: 40 spectral (including FOOOF and ROI-based power values), 3 complexity metrics, and 8 PAC-related features.

2.5. Statistical analysis

All statistical analyses were performed using a combination of R and custom Python scripts. We first assessed the distribution of each variable by visual inspection of quantile–quantile (Q–Q) plots and formal testing with the Kolmogorov–Smirnov (K–S) test. For normally distributed variables, parametric tests were used: independent or paired t-tests for two-group comparisons, and one-way ANOVA or ANCOVA for comparisons across more than two groups or when adjusting for covariates. For non-normally distributed variables, non-parametric alternatives were applied, including the Wilcoxon–Mann–Whitney and Kruskal–Wallis tests.

For categorical variables, the chi-square test of independence was used.

Group differences in plasma biomarkers (p-tau217, p-tau181, Aβ42/40, p-tau217/ Aβ42) were controlled for age, sex, and creatinine.

EEG group comparisons focused on global (electrode-averaged) features; ROI-based features were computed but reserved for machine learning analyses.

To explore associations between EEG features and plasma biomarkers, we first computed Spearman's rank correlation coefficients between EEG features and individual plasma biomarkers (p-tau217, p-tau181, p-tau217/Aβ42, and Aβ42/40 ratio) in the whole sample, applying false discovery rate (FDR) correction for multiple comparisons. To reduce dimensionality and account for potential collinearity among biomarkers, we then performed principal component analysis (PCA) on the standardized plasma dataset. Components with eigenvalues greater than one were retained, and their scores were subsequently correlated with EEG features using Spearman correlation.

To explore potential stage-specific relationships between EEG markers and AD pathology, we conducted Spearman correlation analyses between EEG features that showed significant group differences and plasma p-tau217 levels, separately within each diagnostic group (SCD, AD-MCI, AD-DEM). Given the exploratory nature of this analysis and the a priori focus on p-tau217 as the most established biomarker of AD pathology, no correction for multiple comparisons was applied at this stage, in order to preserve sensitivity in this hypothesis-generating step.

For machine learning analyses, both classification and regression models were implemented in Python using the scikit-learn library to predict p-tau217 plasma positivity and continuous p-tau217 levels using

the same EEG feature set. The classification outcome was p-tau217 plasma positivity, defined using the 0.23 pg/mL threshold from our previous work, (Cecchetti et al., 2024) which demonstrated excellent discriminative performance in reflecting CSF A + and A+/T + status in a real-world setting. We evaluated multiple classification algorithms, including logistic regression, support vector machines (SVM), and random forests, as well as regression algorithms, including stepwise linear regression, ridge regression, and random forest regression. Hyperparameters were optimized using grid search with F1-score maximization within the cross-validation framework. For random forest models, the number of trees, maximum tree depth, minimum samples per split, and number of features considered at each split were tuned. For support vector machines and regularized logistic regression models, regularization and kernel-specific parameters were optimized. All models were trained on the full set of EEG features. To minimize overfitting and ensure robust evaluation, model performance was estimated using leave-one-out cross-validation (LOOCV). Performance metrics included the area under the receiver operating characteristic curve (AUC-ROC), sensitivity, and specificity for classification models, and R-squared and root mean squared error (RMSE) for regression models. Ninety-five percent confidence intervals for AUC were obtained using bootstrap resampling (1,000 iterations). To interpret variable contributions in the classification models, feature importance was estimated using permutation-based methods (varImp library), and model interpretability was enhanced using SHAP (SHapley Additive exPlanations) values, which quantified the direction and magnitude of each feature's contribution to the prediction. (Lundberg and Unified, 2017).

All statistical tests were two-tailed, and significance was set at $p < 0.05$ unless otherwise specified.

3. RESULTS

3.1. Sample characteristics

A total of 165 participants were included: 37 SCD, 51 AD-MCI, 40 AD-DEM, and 36 HC (Table 1).

Groups differed slightly in age (Table 1). Both AD-MCI and AD-DEM participants were significantly older than those in the SCD group, and AD-MCI were also older than HC. No significant age difference was found between AD-DEM and HC (Table 1).

MMSE scores differed significantly between patient groups, between AD-MCI and HC and between AD-DEM and HC (mean ± SD: HC = 28.5 ± 2.4; SCD = 28.8 ± 1.2; AD-MCI = 26.1 ± 2.4; AD-DEM = 21.7 ± 3.9). No significant differences were found between HC and SCD.

No significant group differences emerged for education, nor for gender distribution.

ApoE genotype was available in a subset of participants. Among those with available data, 22/36 (61 %) AD-DEM patients, 15/44 (34 %) AD-MCI patients, and 20/30 (67 %) SCD individuals were ε4 non-carriers. A chi-square test revealed a significant difference in ε4 carrier distribution across groups, with AD-MCI patients showing a higher proportion of ε4 carriers compared to both SCD and AD-DEM.

3.2. Plasma biomarkers of AD

Significant effects of diagnosis were found for all biomarkers, although with different patterns. Results are summarized in Fig. 1.

For p-tau217 and p-tau217/Aβ42, both AD-MCI and AD-DEM patients showed higher plasma levels compared to the SCD group, with no difference between the two AD groups. Similarly, Aβ42/40 ratios were lower in both AD-MCI and AD-DEM compared to SCD, again without differences between the two AD groups. A different pattern was observed for p-tau181, where only AD-DEM patients showed elevated levels compared to SCD, while AD-MCI did not significantly differ from either group. Notably, in this model creatinine emerged as a significant covariate, whereas age and sex did not.

Among patients, 85 out of 128 (66 %) had p-tau217 levels above the established threshold,(6) including 47 out of 51 AD-MCI, 38 out of 40 AD-DEM, and 2 SCD cases out of 37. Notably, all AD-MCI/AD-DEM patients with sub-threshold p-tau217 levels (n = 6; 4 AD-MCI and 2 AD-DEM) had evidence of AD pathology based on CSF or amyloid-PET, supporting the accuracy of clinical diagnosis.

3.3. EEG features analysis

3.3.1. Global relative power analysis

Group differences in global theta and alpha power were significant. Full statistics are reported in Fig. 2.

Theta power progressively increased from HC and SCD to AD-MCI and AD-DEM, while alpha power decreased along the same trajectory. Post hoc comparisons showed higher theta power in AD-DEM and AD-MCI versus HC and SCD and significantly reduced alpha power in AD-DEM compared to both HC and SCD. Relative power in other frequency bands did not show significant group effects.

3.3.2. Fooof-derived spectral parameters

Both peak amplitude and peak frequency differed across groups. Full pairwise statistics and distributional details are reported in Fig. 2. AD-MCI and AD-DEM participants showed lower FOOOF peak amplitude and frequency compared to HC. Notably, AD-DEM patients also showed reduced peak frequency relative to SCD. No significant difference was observed between AD-MCI and AD-DEM for either parameter.

Table 1
Demographic and clinical characteristics of the sample across diagnostic groups.

	HC	SCD	AD-MCI	AD-DEM	p-value
N	36	37	51	40	
Demographic and general clinical variables					
Age [years]	64.5 ± 8.49 (35.1–82.3)	64.8 ± 10.9 (46.3–85.6)	74.0 ± 6.1 (55.0–83.5)	72.7 ± 7.9 (53.2–84.2)	**0.001**
Sex [Men/Women]	20/16	21/16	22/29	16/24	0.30
MMSE	28.5 ± 2.4(25.0–30.0)	28.8 ± 1.2(25.0–30.0)	26.1 ± 2.4 (20.0–30.0)	21.7 ± 3.9 (18.0–29.0)	**<0.001**
Education [years]	13.1 ± 4.1 (5.00–18.00)	13.3 ± 4.3(5.00–18.00)	12.6 ± 5.6 (3.0–29.0)	11.8 ± 5.1 (3.00–18.00)	0.15
ApoE4 [non-carriers/total]	–	20/30 (66.7 %)	15/44 (34.1 %)	22/36 (61.1 %)	**0.01**
Plasma biomarkers					
Plasma p-tau217 [pg/mL]	–	0.13 ± 0.09 (0.06–0.55)	0.68 ± 0.40 (0.10–2.06)	0.94 ± 0.55 (0.15–1.95)	**<0.001**
Plasma p-tau181 [pg/mL]	–	1.44 ± 1.07 (0.520–5.47)	2.38 ± 1.12 (0.840–7.08)	2.88 ± 1.14 (1.33–5.33)	**<0.001**
Plasma Aβ-42/40	–	0.090 ± 0.014 (0.067–0.118)	0.074 ± 0.0108 (0.054–0.113)	0.076 ± 0.011 (0.053–0.099)	**<0.001**
Plasma p-tau217/Aβ-42	–	0.005 ± 0.003 (0.002–0.019)	0.037 ± 0.046 (0.003–0.328)	0.041 ± 0.028 (0.008–0.148)	**<0.001**

Values are frequencies (%) or means ± standard deviations (min/max). The level of significance was set at $p < 0.05$ and refers to ANOVA or ANCOVA tests, followed by post-hoc pairwise comparisons, or to Chi-square test (see the main text for further details). Significant comparisons are highlighted in bold. Abbreviations: AD-DEM = mild dementia due to Alzheimer's disease; AD-MCI = mild cognitive impairment due to Alzheimer's disease; ApoE = Apolipoprotein E gene; HC = healthy controls; MMSE = Mini-Mental State Examination; SCD = subjective cognitive decline.

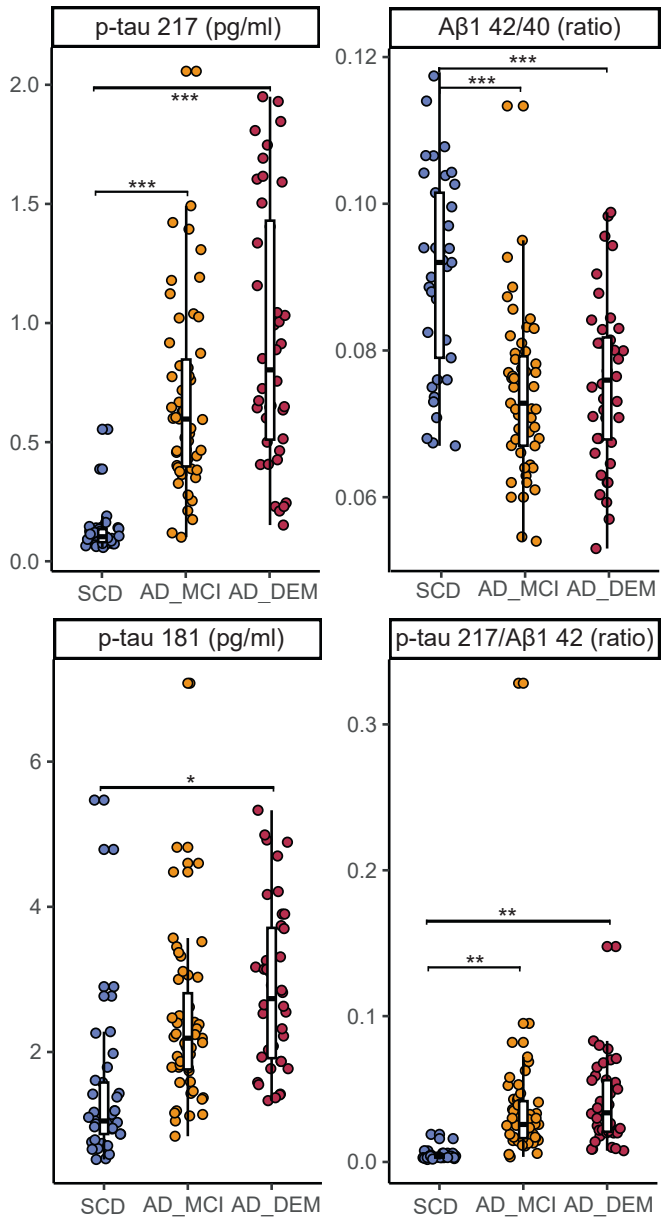

Fig. 1. Plasma concentrations of Alzheimer's disease (AD) biomarkers (p-tau217, p-tau181, Aβ42/40 ratio, and p-tau217/Aβ42 ratio) across diagnostic groups. Group differences were assessed using ANCOVA, adjusting for age, sex, and creatinine. Boxplots represent interquartile ranges, with medians indicated by horizontal lines and whiskers extending to ± 1.5 times the interquartile range. Abbreviations: AD-DEM = mild dementia due to AD; AD-MCI = mild cognitive impairment due to AD; SCD = subjective cognitive decline; * = $p < 0.05$; ** = $p < 0.01$; *** = $p \leq 0.001$.

3.3.3. Global Phase–Amplitude coupling (PAC)

Overall PAC differed significantly across diagnostic groups. Detailed statistics are reported in Fig. 2. AD-DEM and AD-MCI patients showed reduced PAC values compared to SCD, with significant differences observed for both comparisons. No significant differences were found between AD groups and HC, nor between HC and SCD.

3.3.4. EEG complexity metrics

Multiscale Entropy (MSE), Higuchi's Fractal Dimension, and Lempel-Ziv Complexity were computed for each subject at the global level. None of these metrics yielded statistically significant differences across diagnostic groups.

3.4. EEG – Plasma biomarker correlations

We first tested whether EEG features correlated with individual plasma biomarkers or with a composite index derived from PCA of plasma biomarkers in the whole sample. A weak positive correlation was found between theta power and the first principal component (PC1) of the plasma dataset ($r = 0.31$, $p < 0.001$), while PAC showed a weak negative association ($r = –0.17$, $p = 0.040$). However, none of these associations survived correction for multiple testing with the full EEG features dataset.

Correlation analyses stratified by diagnostic groups revealed that, in the AD-DEM group, global theta power was positively associated with p-tau217 levels, while global alpha power showed an inverse correlation (Fig. 3). In the AD-MCI group, a positive correlation was again found between theta power and p-tau217, while alpha power did not show a significant association. In the SCD group, no significant associations were observed between theta or alpha power and p-tau217.

No significant associations were observed between EEG features and other plasma biomarkers, including p-tau181 and the Aβ42/40 ratio.

No significant associations were found between p-tau217 and PAC or FOOOF-derived spectral parameters in any diagnostic subgroup.

3.5. Eeg-based prediction of plasma p-tau217 status and levels

Linear regression analyses did not show a significant relationship between EEG features and continuous plasma p-tau217 levels. Alternative regression models, including ridge regression and random forest regression, similarly showed limited predictive performance across all tested algorithms (Supplementary Fig. 1), with explained variance remaining low ($R^2 \leq 0.26$), indicating limited robustness.

In contrast, classification models aimed at predicting plasma p-tau217 positivity demonstrated more robust performance. Among the tested algorithms, the random forest model achieved the highest cross-validated AUC and was therefore selected for subsequent analyses.

The final random forest model achieved an area under the receiver operating characteristic curve (AUC-ROC) of 0.75, with a sensitivity of 0.73, specificity of 0.62, and overall accuracy of 0.68. The ROC curve and its 95 % confidence intervals, obtained via bootstrap resampling (1,000 iterations), are shown in Fig. 4 (panel a).

To further characterize model robustness, we assessed the sensitivity of the random forest classifier to the number of input EEG features. Classification accuracy reached a plateau when approximately 15–20 features were included, indicating that a reduced subset of top-ranked features was sufficient to achieve performance comparable to the full feature set (Supplementary Fig. 2).

Feature importance was subsequently computed for the final model, and the top 20 contributing features were identified (Fig. 4, panel b). Their relative impact and directionality were interpreted using permutation-based variable importance and SHAP (SHapley Additive exPlanations) values, as shown in Fig. 4 (panel c).

4. Discussion

In this study, we combined molecular profiling via plasma biomarkers with functional assessment through 32-channel resting-state EEG in a well-characterized cohort spanning SCD, MCI and mild dementia due to AD.

To our knowledge, this is the first study to examine the association between plasma biomarkers and advanced EEG features in a real-world clinical setting. A distinctive feature of this work is the implementation of a semi-automated EEG preprocessing pipeline, enabling standardized and reproducible signal cleaning and feature extraction. By integrating high-throughput EEG metrics (including spectral, complexity, and cross-frequency coupling measures) into machine learning models, we show that resting EEG can detect cases of pathologically increased p-tau217. This combined approach offers a promising step toward accessible,

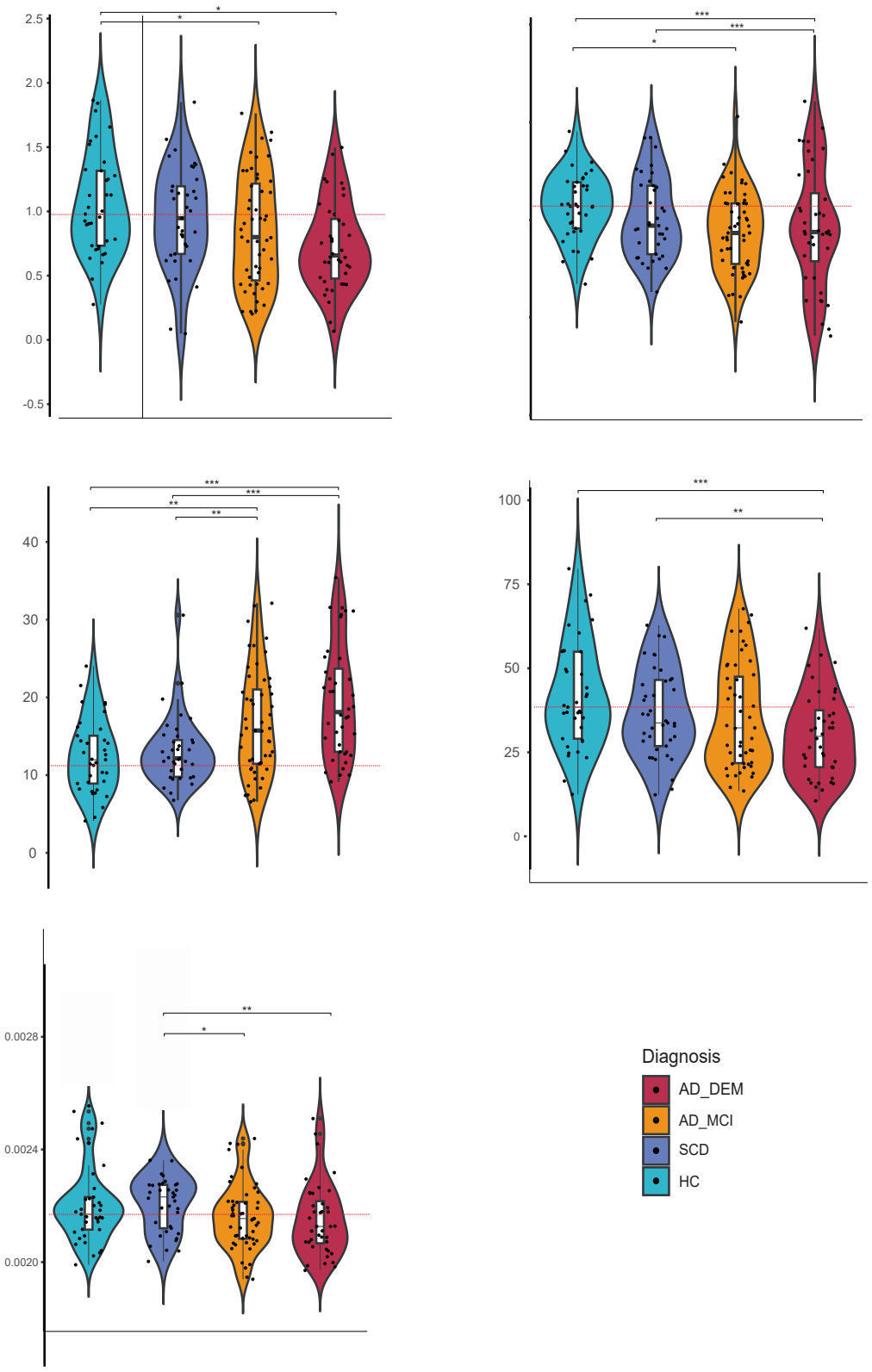

Fig. 2. Global EEG features across diagnostic groups. Group differences were assessed using non-parametric Kruskal–Wallis tests on electrode-averaged measures. Only features showing significant between-group effects are displayed. The red dashed line indicates the median reference value of the healthy control (HC) group. Abbreviations: AD-dem = Alzheimer's disease dementia; AD-MCI = mild cognitive impairment due to Alzheimer's disease; EEG = electroencephalography; FOOOFpeakAmp = amplitude of background activity after detrending for 1/f component; FOOOFpeakFreq = central frequency of background EEG activity identified by the FOOOF algorithm; Global Theta and Global Alpha (band power, average among channels); HC = healthy controls; PAC = phase–amplitude coupling; SCD = subjective cognitive decline; * = $p < 0.05$; ** = $p < 0.01$; *** = $p \leq 0.001$.

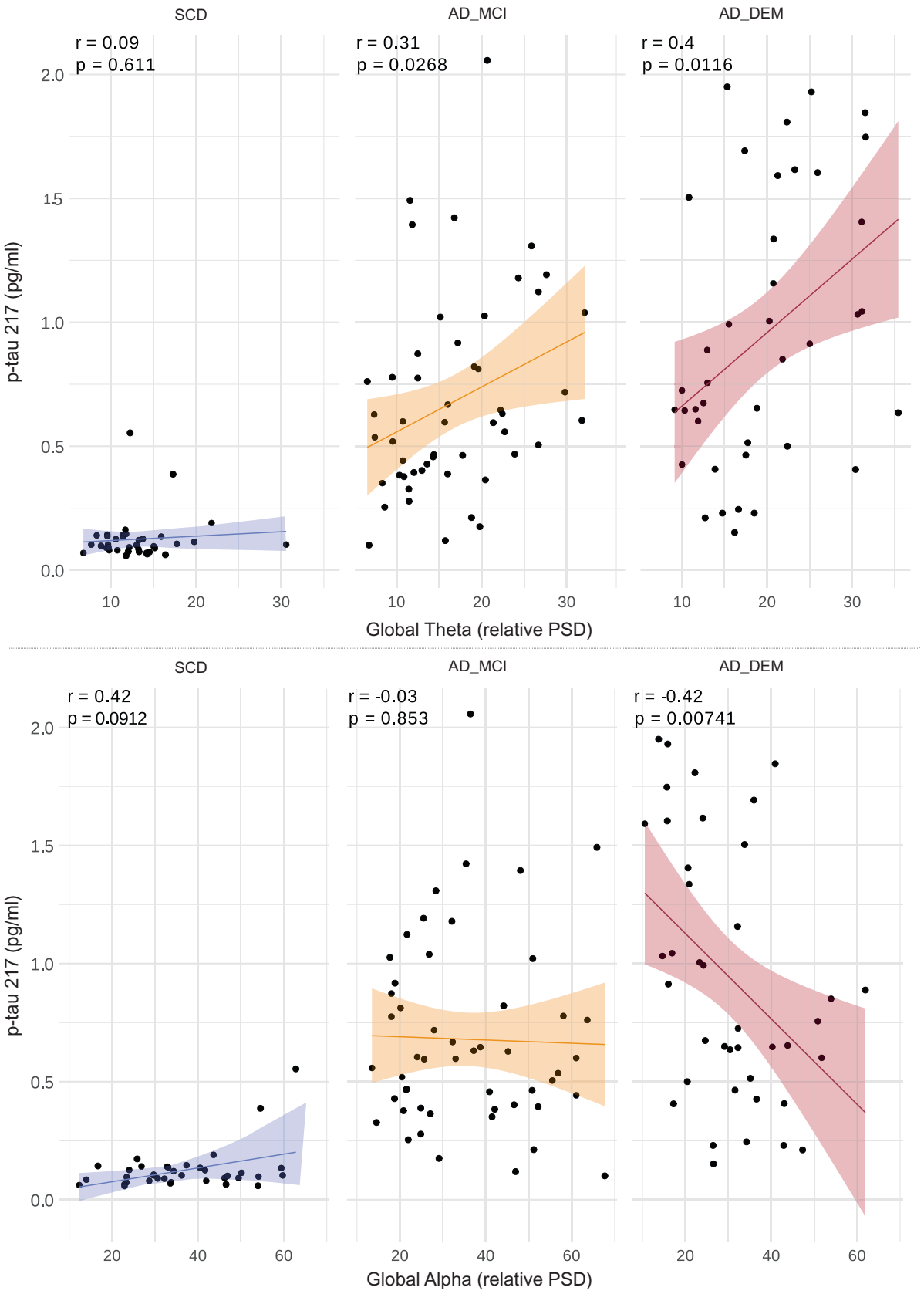

Fig. 3. Correlation between EEG spectral features and plasma p-tau217 levels across diagnostic groups. Scatterplots display the associations between global theta and alpha power and plasma p-tau217 concentration within each diagnostic group (SCD, AD-MCI, AD-DEM). Each point represents an individual patient. Linear regression lines are shown. Correlation values refer to Spearman's rank coefficients. Abbreviations: AD-DEM = Alzheimer's disease dementia; AD-MCI = mild cognitive impairment due to Alzheimer's disease; Global Alpha = alpha power average among channels; Global Theta = theta power average among channels; p-tau217 = plasma phosphorylated tau at threonine 217; SCD = subjective cognitive decline.

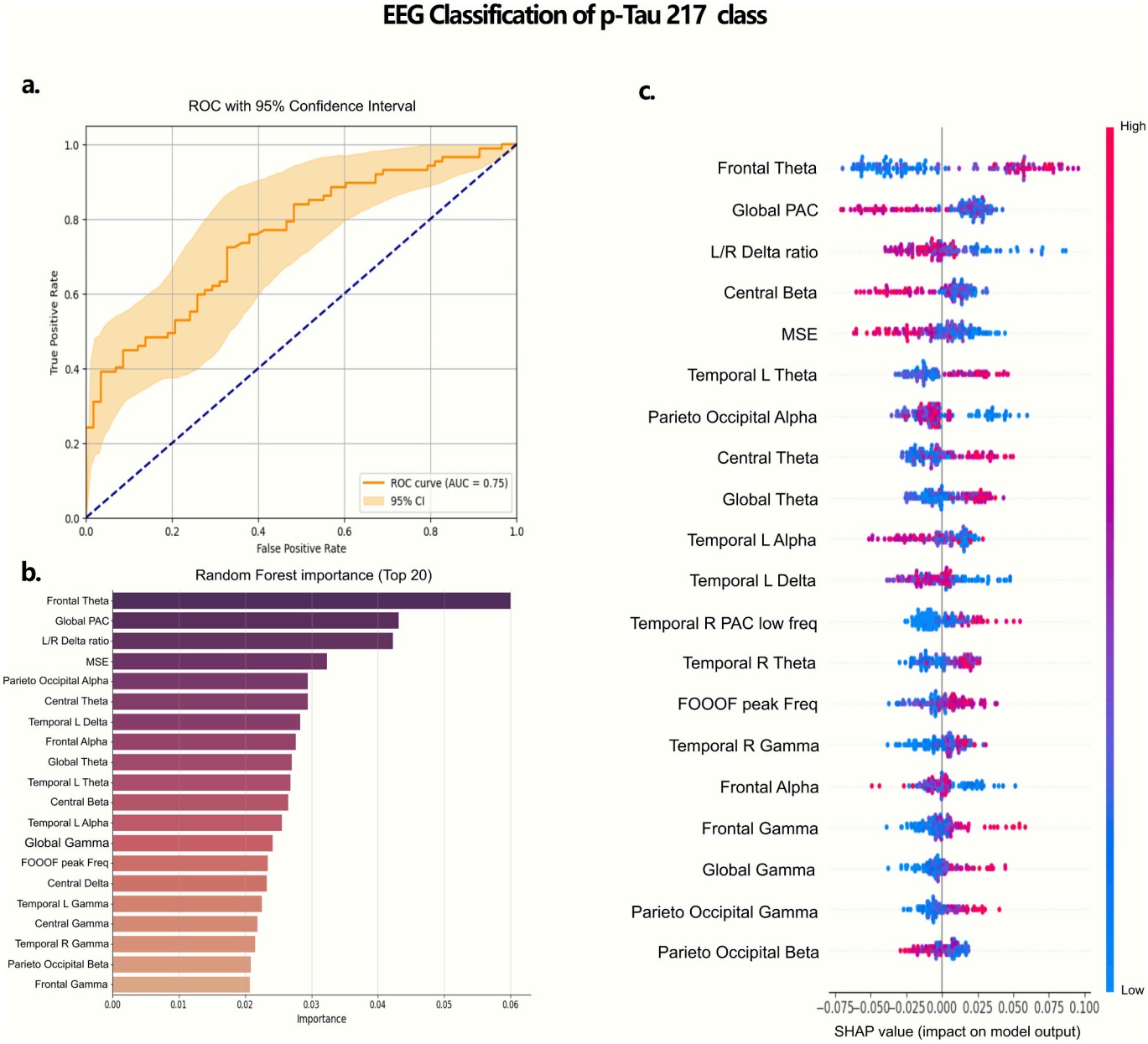

Fig. 4. EEG-based classification of plasma p-tau217 positivity using a random forest model. The classifier was trained to distinguish individuals with p-tau217 levels above the validated threshold (0.23 pg/mL) using all extracted EEG features. (Cecchetti et al., 2024) Model performance was assessed via leave-one-out cross-validation and bootstrap resampling (1,000 iterations). The receiver operating characteristic (ROC) curve is shown, with an area under the curve (AUC) of 0.75, sensitivity of 0.73, specificity of 0.62, and overall accuracy of 0.68 (panel a.). The contribution of the top 20 features was assessed using permutation-based variable importance (VarImp; panel b.) and SHAP (SHapley Additive exPlanations, panel c.) values. Abbreviations: AUC = area under the curve; EEG = electroencephalography; L = Left; R = Right; FOOOFpeakAmp = amplitude of background activity after detrending for the 1/f component; FOOOFpeakFreq = central frequency of background EEG activity identified by the FOOOF algorithm; MSE = multiscale entropy; PAC = Phase–Amplitude Coupling; PAC_low_freq / PAC_high_freq = frequency ranges (theta/gamma) at maximum coupling; ROC = receiver operating characteristic. Frontal, Central, Temporal, and Parieto-Occipital = scalp regions defined as the average of corresponding electrodes from the standard 10–20 montage.

biologically grounded tools for early diagnosis and patient stratification. Ultimately, it may help bridging critical gaps in patient care.

In line with our previous findings and other recent reports, (Cecchetti et al., 2024; Arranz et al., 2023; Bellomo et al., 2024) plasma levels of p-tau217 were significantly elevated in both AD-MCI and AD-DEM patients compared to individuals with SCD, whereas p-tau181 levels were significantly increased mainly in the AD-DEM group. In contrast, Aβ42/40 ratios were reduced across the AD spectrum. Notably, these results were obtained in a new, independent clinical cohort distinct from that analyzed in Cecchetti et al., (Cecchetti et al., 2024) reinforcing the robustness and generalizability of plasma biomarkers in capturing AD-related pathology, even when accounting for potential confounders (e.g., kidney function, age).

A key result from EEG analysis was the confirmation of spectral slowing as a robust EEG signature of AD. We observed progressive increases in low-frequency activity (especially theta) and decreases in alpha power across clinical stages, consistent with the literature. (Cassani et al., 2018; Jeong, 2004) The gradient of slowing (from SCD to AD-DEM) mirrors the progressive synaptic dysfunction observed in AD and replicates findings from our earlier studies. (Cecchetti et al., 2021; Cecchetti et al., 2024) These changes also appeared in our machine learning model as relevant features for classification. Although not

specific to AD, such slowing patterns are well-characterized in the disease and suggest a general loss of network efficiency, serving as a marker of neurodegeneration.

FOOOF-based spectral decomposition provided further insight into the neurophysiological underpinnings of spectral slowing. We found that both FOOOF peak amplitude and peak frequency were significantly reduced in patients with AD-MCI and AD-DEM compared to controls, with the most pronounced reductions observed in the dementia stage. This finding reinforces the notion that slowing in AD primarily reflects a disruption and desynchronization of resting alpha brain activity. These results are consistent with recent work suggesting that EEG slowing in AD might not be merely a byproduct of increased neural noise but reflects genuine disruption in the generation or maintenance of cortical oscillations. (Donoghue et al., 2020) This manifests as a lower central frequency, a reduced 1/f normalized peak, and decreased relative power in the alpha band. Concurrently, there's an increase in theta activity, potentially due to a shift of the posterior dominant rhythm to slower frequencies.

In addition to spectral markers, we explored more sophisticated features including PAC and signal complexity. PAC, which captures cross-frequency interactions such as theta–gamma coupling, was modestly reduced in the AD groups. Although between-group differences were not large, these findings are in line with evidence indicating early disruption of cross-frequency coupling in AD. (Koelewijn et al., 2019).

Initial analyses across the entire cohort did not reveal significant correlations between individual EEG features and plasma biomarkers. Even after dimensionality reduction using PCA, weak associations (such as those between theta power, PAC, and the first principal component) did not survive correction for multiple comparisons.

To further investigate whether disease stage modulates EEG–biomarker relationships, we performed exploratory correlation analyses within diagnostic groups. In both the AD-MCI and AD-DEM groups, global theta power was positively associated with plasma p-tau217 levels, with a stronger effect observed in the AD-DEM group. A negative association involving alpha power emerged only in AD-DEM, whereas no significant correlations were observed in AD-MCI at the alpha band, nor in SCD at either frequency band.

These findings support the hypothesis that EEG–biomarker associations emerge in a stage-dependent manner, becoming detectable beyond a critical threshold of pathological burden, and align with the concept of differential temporal sensitivity of EEG rhythms, whereby theta alterations may index earlier synaptic dysfunction and alpha slowing may reflect more advanced neurodegeneration. (Cecchetti et al., 2021; Cecchetti et al., 2024) While previous studies have reported associations between EEG slowing and CSF or amyloid-PET biomarkers, (Musaeus et al., 2018; Stomrud et al., 2010) this is, to our knowledge, the first study to demonstrate stage-specific correlations between EEG rhythms and plasma p-tau217 levels in a memory clinic cohort.

Importantly, no significant associations between EEG features and plasma p-tau217 were observed within the SCD group. In contrast, stage-specific relationships emerged in symptomatic phases, with distinct EEG–biomarker coupling patterns in AD-MCI and AD-DEM. This supports the notion that measurable EEG correlates of tau-related pathology become more evident with increasing disease burden. Although exploratory, these findings are compatible with emerging evidence suggesting non-linear neurophysiological trajectories along the Alzheimer's disease continuum, in which both amyloid and tau pathology have been associated with non-monotonic changes in brain network organization and function. (Mijalkov et al., 2023) In this context, EEG markers may capture stage-dependent functional consequences of pathology that are not adequately described by global linear models. Accordingly, we favored stratified analyses over a single interaction-based regression approach, in order to explore within-stage relationships without imposing a uniform linear interaction across diagnostic groups.

The EEG-based machine learning model achieved an AUC of 0.75 in identifying individuals with p-tau217 positivity using EEG features alone. This is a promising result given the inherent complexity of both EEG signals and plasma biomarker levels. Despite the lack of strong linear correlations between EEG and plasma biomarkers in the entire cohort, EEG features robustly predicted p-tau217 positivity, used here as a proxy of underlying amyloid and tau pathology. This supports the hypothesis that EEG captures distinct functional consequences of molecular pathology, offering complementary information on network-level disruption in AD.

However, when attempting to predict continuous plasma p-tau217 values across the whole cohort, machine learning models failed to achieve meaningful performance. This likely reflects the stage-dependent and non-linear nature of EEG–biomarker relationships, whereby EEG features may be more sensitive to threshold-like functional changes than to continuous variations in plasma biomarker levels.

An important aspect in interpreting EEG–proteinopathy relationships is therefore the choice of the reference biomarker. PET imaging provides high spatial specificity and enables topographical mapping of amyloid or tau burden, which can be leveraged in EEG source-level analyses and has been shown to improve pathological detection, including in pre-dementia stages. (Kim et al., 2023; Szelies et al., 1992) In contrast, plasma biomarkers offer a complementary and scalable approach. Although they lack spatial resolution, they are minimally invasive, easily repeatable, and well suited for outpatient and real-world clinical settings. In this context, plasma p-tau217 represents a practical tool to investigate stage-dependent functional consequences of Alzheimer's pathology on brain activity. Future studies integrating PET imaging and plasma biomarkers will be essential to clarify how regional protein deposition relates to EEG alterations across disease stages.

Notably, many of the most influential predictors in the classification model overlapped with those showing significant group-level differences. Alpha and theta relative power appeared in 8 of the top 20 predictors, reinforcing their value as core features of EEG slowing along the AD continuum. Interestingly, while theta–gamma PAC showed only marginal significance in direct group comparisons, it emerged as the second most important feature in the classifier. This apparent dissociation suggests that PAC may capture individual-level alterations related to AD pathology that are not fully reflected by mean group differences. Given the established role of theta-gamma coupling in memory processes, and experimental evidence indicating that amyloid and tau pathology disrupt PAC through dysfunction of parvalbumin-positive (PV +) interneurons (which coordinate gamma oscillations and temporal integration of neural activity (Palop and Mucke, 2016) our findings support the interpretation that reduced PAC in AD-MCI and AD-DEM may reflect early circuit-level disintegration, particularly within limbic networks, detectable through non-invasive EEG.

MSE was also selected as one of the most discriminative features in the random forest classifier. Specifically, lower MSE values were associated with p-tau217-positive individuals. This suggests that entropy, while not useful for group-level discrimination in this sample, may reflect individual-level differences in brain signal irregularity linked to underlying pathology. The inclusion of MSE in the classifier resonates with prior studies showing entropy reduction in AD and highlights the potential of complexity metrics in multivariate predictive models. (Babiloni et al., 2017).

Another relevant observation is that most of the influential EEG features exhibited left-hemispheric dominance, in line with previous neuroimaging and electrophysiological studies in AD. (Loewenstein et al., 1989; Yang et al., 2017) This asymmetry may reflect the well-documented lateralization of neurodegenerative processes, particularly in early disease stages. Among the most discriminative features, we identified increased asymmetry in delta activity, which may signal early lateralized network degeneration. (Loewenstein et al., 1989) Reduced beta power also emerged as a relevant marker, possibly indicating decreased cortical excitability and impaired sensorimotor or cognitive

synchronization. (Walters et al., 2025) In contrast, increased gamma power—though less commonly emphasized—may reflect abnormal synchronization phenomena, compensatory overactivation, or pathological cross-frequency coupling, all of which can disrupt large-scale network dynamics and reduce signal complexity. (Wang et al., 2017).

While these results are encouraging, several limitations must be noted. First, the study is cross-sectional and monocentric, limiting generalizability and precluding causal inference. Longitudinal data will be essential to determine whether EEG features can predict biomarker conversion or clinical progression. Second, although the classifier showed promising accuracy, validation in larger and more heterogeneous cohorts is necessary. Future work will aim to establish cross-site generalizability and validate performance across different EEG acquisition systems. Third, despite the clinical appeal of EEG as a scalable and cost-effective tool, the translation of some advanced quantitative metrics into routine practice remains challenging. While conventional spectral measures (e.g., band power) are readily obtainable in standard clinical EEG settings, features such as signal complexity and PAC currently require specialized expertise and custom scripts, which may limit immediate implementation and reproducibility across sites. To mitigate these issues, future work should prioritize standardization of data organization (e.g., EEG-BIDS), harmonization of feature-extraction procedures, and the development of fully automated and portable workflows (e.g., containerized pipelines). These steps are expected to progressively improve reproducibility and facilitate broader clinical adoption of advanced qEEG markers.

This study shows that EEG can detect functional brain alterations associated with plasma-defined AD pathology. EEG and plasma biomarkers likely capture complementary aspects of the disease: the former reflecting functional network disruption, the latter indexing molecular pathology. Our findings suggest that once amyloid and tau pathology cross pathological thresholds, EEG may reveal their functional footprint through changes in spectral dynamics, cross-frequency coupling, and signal complexity. While EEG features did not predict absolute p-tau217 values in the whole sample, they accurately identified individuals above the established positivity cutoff. This supports the notion that EEG reflects categorical, rather than continuous, shifts in brain function associated with AD pathology. Moreover, stage-specific associations with theta and alpha activity highlight EEG's potential to track different phases of disease progression. EEG may thus offer a scalable, biologically grounded tool for early diagnosis, patient stratification and, potentially, therapeutic response, particularly where access to biomarkers is limited.

CRediT authorship contribution statement

Giordano Cecchetti: Writing – review & editing, Writing – original draft, Investigation, Formal analysis, Data curation, Conceptualization. **Jacopo Lanzone:** Writing – review & editing, Writing – original draft, Investigation, Formal analysis, Data curation, Conceptualization. **Luca Zanchi:** Writing – review & editing, Investigation, Formal analysis. **Giulia Rugarli:** Writing – review & editing, Investigation. **Silvia Basaia:** Writing – review & editing, Investigation, Formal analysis, Data curation. **Marco Cursi:** Writing – review & editing, Investigation, Formal analysis, Data curation. **Federico Coraglia:** Writing – review & editing, Investigation. **Edoardo G. Spinelli:** Writing – review & editing, Investigation, Formal analysis. **Alma Ghirelli:** Writing – review & editing, Investigation. **Elisa Canu:** Writing – review & editing, Investigation, Formal analysis. **Elisa Sibilla:** Writing – review & editing, Investigation. **Francesca Caso:** Writing – review & editing, Investigation. **Roberto Santangelo:** Writing – review & editing, Investigation. **Davide Curti:** Writing – review & editing, Investigation. **Giovanna Franca Fanelli:** Writing – review & editing, Investigation. **Anna Bellini:** Writing – review & editing, Investigation, Formal analysis. **Giuseppe Magnani:** Writing – review & editing, Investigation. **Federica Agosta:** Writing – review & editing, Writing – original draft, Investigation, Formal analysis, Data curation, Conceptualization. **Massimo Filippi:** Writing – review & editing, Supervision, Data curation, Conceptualization.

Funding

This research did not receive any specific grant from funding agencies in the public, commercial, or not-for-profit sectors.

Declaration of competing interest

The authors declare the following financial interests/personal relationships which may be considered as potential competing interests: G. Cecchetti has received speaker honoraria from Neopharmed Gentili and Eli Lilly. J. Lanzone has nothing to disclose. L. Zanchi has nothing to disclose. G. Rugarli has nothing to disclose. S. Basaia has nothing to disclose. M. Cursi has nothing to disclose. F. Coraglia has nothing to disclose. E.G. Spinelli has nothing to disclose. A. Ghirelli has received speaker honoraria from Eli Lilly. E. Canu has nothing to disclose. E. Sibilla has nothing to disclose. F. Caso has nothing to disclose. R. Santangelo has nothing to disclose. D. Curti has nothing to disclose. G.F. Fanelli has nothing to disclose. A. Bellini has nothing to disclose. G. Magnani has nothing to disclose. F. Agosta is Associate Editor of *NeuroImage: Clinical*, has received speaker honoraria from Biogen Idec, Roche, Eli Lilly, GE Healthcare and Bristol Myers Squibb, and receives or has received research supports from the Italian Ministry of Health, the Italian Ministry of University and Research, AriSLA (Fondazione Italiana di Ricerca per la SLA), the European Research Council (ERC), the EU Joint Programme – Neurodegenerative Disease Research (JPND), and Foundation Research on Alzheimer Disease (France). M. Filippi is Editor-in-Chief of the *Journal of Neurology*, Associate Editor of *Human Brain Mapping*, *Neurological Sciences,* and *Radiology*; received compensation for consulting services from Almirall, Biogen, Bristol-Myers Squibb, Eli Lilly, Merck, Novartis, Roche, Sanofi; speaking activities from Amgen, Bayer, Biogen, Bristol-Myers Squibb, Celgene, Chiesi Italia SpA, Eisai, Eli Lilly, Fujirebio, Genzyme, Janssen, Merck, Neopharmed Gentili, Neuraxpharm, Novartis, Novo Nordisk, Roche, Sanofi, Takeda; participation in Advisory Boards for Alexion, Biogen, Bristol-Myers Squibb, Eli Lilly, GE Healthcare Ltd, Merck, Neuraxpharm, Novartis, Roche, Sandoz, Sanofi, Takeda; scientific direction of educational events for Biogen, Merck, Roche, Celgene, Bristol-Myers Squibb, Lilly, Novartis, Sanofi-Genzyme; he receives research support from Biogen Idec, Merck-Serono, Novartis, Roche, the Italian Ministry of Health, the Italian Ministry of University and Research, and Fondazione Italiana Sclerosi Multipla.

Acknowledgments

We express our gratitude to Fujirebio Italia for their invaluable support in providing part of the research kits free of charge for our scientific investigation.

Appendix A. Supplementary data

Supplementary data to this article can be found online at https://doi.org/10.1016/j.nicl.2026.103947.

Data availability

Data will be made available on request.

References

Scheltens, P., De Strooper, B., Kivipelto, M., Holstege, H., Chetelat, G., Teunissen, C.E., et al., 2021. Alzheimer's disease. Lancet 397 (10284), 1577–1590.

Jack Jr., C.R., Bennett, D.A., Blennow, K., Carrillo, M.C., Dunn, B., Haeberlein, S.B., et al., 2018. NIA-AA Research Framework: Toward a biological definition of Alzheimer's disease. Alzheimers Dement. 14 (4), 535–562.
Jack Jr., C.R., Andrews, J.S., Beach, T.G., Buracchio, T., Dunn, B., Graf, A., et al., 2024. Revised criteria for diagnosis and staging of Alzheimer's disease: Alzheimer's Association Workgroup. Alzheimers Dement. 20 (8), 5143–5169.
Palmqvist, S., Janelidze, S., Quiroz, Y.T., Zetterberg, H., Lopera, F., Stomrud, E., et al., 2020. Discriminative Accuracy of Plasma phospho-tau217 for Alzheimer Disease vs Other Neurodegenerative Disorders. J. Am. Med. Assoc. 324 (8), 772–781.
Janelidze, S., Berron, D., Smith, R., Strandberg, O., Proctor, N.K., Dage, J.L., et al., 2021. Associations of Plasma Phospho-Tau217 levels with Tau Positron Emission Tomography in Early Alzheimer Disease. JAMA Neurol. 78 (2), 149–156.
Cecchetti, G., Agosta, F., Rugarli, G., Spinelli, E.G., Ghirelli, A., Zavarella, M., et al., 2024. Diagnostic accuracy of automated Lumipulse plasma pTau-217 in Alzheimer's disease: a real-world study. J. Neurol. 271 (10), 6739–6749.
Dauwels, J., Srinivasan, K., Ramasubba Reddy, M., Musha, T., Vialatte, F.B., Latchoumane, C., et al., 2011. Slowing and loss of Complexity in Alzheimer's EEG: two Sides of the same Coin? Int. J. Alzheimers Dis. 2011, 539621.
Smailovic, U., Koenig, T., Kareholt, I., Andersson, T., Kramberger, M.G., Winblad, B., et al., 2018. Quantitative EEG power and synchronization correlate with Alzheimer's disease CSF biomarkers. Neurobiol. Aging 63, 88–95.
Cecchetti, G., Agosta, F., Basaia, S., Cividini, C., Cursi, M., Santangelo, R., et al., 2021. Resting-state electroencephalographic biomarkers of Alzheimer's disease. Neuroimage Clin. 31, 102711.
Cecchetti, G., Agosta, F., Canu, E., Basaia, S., Rugarli, G., Curti, D.G., et al., 2024. Analysis of individual alpha frequency in a large cohort from a tertiary memory center. Eur. J. Neurol. 31 (10), e16424.
Cecchetti, G., Basaia, S., Canu, E., Cividini, C., Cursi, M., Caso, F., et al., 2024. EEG Correlates in the 3 Variants of Primary Progressive Aphasia. Neurology 102 (3), e207993.
Chetty, C.A., Bhardwaj, H., Kumar, G.P., Devanand, T., Sekhar, C.S.A., Akturk, T., et al., 2024. EEG biomarkers in Alzheimer's and prodromal Alzheimer's: a comprehensive analysis of spectral and connectivity features. Alzheimers Res. Ther. 16 (1), 236.
Nuwer, M.R., Comi, G., Emerson, R., Fuglsang-Frederiksen, A., Guerit, J.M., Hinrichs, H., et al., 1998. IFCN standards for digital recording of clinical EEG. International Federation of Clinical Neurophysiology. Electroencephalogr. Clin. Neurophysiol. 106 (3), 259–261.
Chang, C.Y., Hsu, S.H., Pion-Tonachini, L., Jung, T.P., 2020. Evaluation of Artifact Subspace Reconstruction for Automatic Artifact Components Removal in Multi-Channel EEG Recordings. I.E.E.E. Trans. Biomed. Eng. 67 (4), 1114–1121.
Pion-Tonachini, L., Kreutz-Delgado, K., Makeig, S., 2019. ICLabel: an automated electroencephalographic independent component classifier, dataset, and website. Neuroimage 198, 181–197.
Eric L. MNE-Python 2024 [updated December 18, 2024. Available from: https://zenodo.org/records/14519545.
Donoghue, T., Haller, M., Peterson, E.J., Varma, P., Sebastian, P., Gao, R., et al., 2020. Parameterizing neural power spectra into periodic and aperiodic components. Nat. Neurosci. 23 (12), 1655–1665.
Canolty, R.T., Edwards, E., Dalal, S.S., Soltani, M., Nagarajan, S.S., Kirsch, H.E., et al., 2006. High gamma power is phase-locked to theta oscillations in human neocortex. Science 313 (5793), 1626–1628.
Dupre la Tour, T., Tallot, L., Grabot, L., Doyere, V., van Wassenhove, V., Grenier, Y., et al., 2017. Non-linear auto-regressive models for cross-frequency coupling in neural time series. PLoS Comput. Biol. 13 (12), e1005893.
Makowski, D., Pham, T., Lau, Z.J., Brammer, J.C., Lespinasse, F., Pham, H., et al., 2021. NeuroKit2: a Python toolbox for neurophysiological signal processing. Behav. Res. Methods 53 (4), 1689–1696.
Lundberg SML, S. A Unified Approach to Interpreting Model Predictions. 2017.
Arranz, J., Zhu, N., Rubio-Guerra, S., Rodriguez-Baz, I., Ferrer, R., Carmona-Iragui, M., et al., 2023. Diagnostic performance of plasma pTau 217, pTau 181, Abeta 1-42 and Abeta 1-40 in the LUMIPULSE automated platform for the detection of Alzheimer disease. Res Sq.
Bellomo, G., Bayoumy, S., Megaro, A., Toja, A., Nardi, G., Gaetani, L., et al., 2024. Fully automated measurement of plasma Abeta42/40 and p-tau181: Analytical robustness and concordance with cerebrospinal fluid profile along the Alzheimer's disease continuum in two independent cohorts. Alzheimers Dement. 20 (4), 2453–2468.
Cassani, R., Estarellas, M., San-Martin, R., Fraga, F.J., Falk, T.H., 2018. Systematic Review on Resting-State EEG for Alzheimer's Disease Diagnosis and Progression Assessment. Dis. Markers 2018, 5174815.
Jeong, J., 2004. EEG dynamics in patients with Alzheimer's disease. Clin. Neurophysiol. 115 (7), 1490–1505.
Koelewijn, L., Lancaster, T.M., Linden, D., Dima, D.C., Routley, B.C., Magazzini, L., et al., 2019. Oscillatory hyperactivity and hyperconnectivity in young APOE-varepsilon4 carriers and hypoconnectivity in Alzheimer's disease. Elife 8.
Musaeus, C.S., Engedal, K., Hogh, P., Jelic, V., Morup, M., Naik, M., et al., 2018. EEG Theta Power is an Early Marker of Cognitive Decline in Dementia due to Alzheimer's Disease. J. Alzheimers Dis. 64 (4), 1359–1371.
Stomrud, E., Hansson, O., Minthon, L., Blennow, K., Rosen, I., Londos, E., 2010. Slowing of EEG correlates with CSF biomarkers and reduced cognitive speed in elderly with normal cognition over 4 years. Neurobiol. Aging 31 (2), 215–223.
Mijalkov, M., Vereb, D., Canal-Garcia, A., Hinault, T., Volpe, G., Pereira, J.B., et al., 2023. Nonlinear changes in delayed functional network topology in Alzheimer's disease: relationship with amyloid and tau pathology. Alzheimers Res. Ther. 15 (1), 112.
Kim, N.H., Park, U., Yang, D.W., Choi, S.H., Youn, Y.C., Kang, S.W., 2023. PET-validated EEG-machine learning algorithm predicts brain amyloid pathology in pre-dementia Alzheimer's disease. Sci. Rep. 13 (1), 10299.
Szelies, B., Grond, M., Herholz, K., Kessler, J., Wullen, T., Heiss, W.D., 1992. Quantitative EEG mapping and PET in Alzheimer's disease. J. Neurol. Sci. 110 (1–2), 46–56.
Palop, J.J., Mucke, L., 2016. Network abnormalities and interneuron dysfunction in Alzheimer disease. Nat. Rev. Neurosci. 17 (12), 777–792.
Babiloni, C., Del Percio, C., Lizio, R., Noce, G., Cordone, S., Lopez, S., et al., 2017. Abnormalities of cortical neural synchronization mechanisms in patients with dementia due to Alzheimer's and Lewy body diseases: an EEG study. Neurobiol. Aging 55, 143–158.
Loewenstein, D.A., Barker, W.W., Chang, J.Y., Apicella, A., Yoshii, F., Kothari, P., et al., 1989. Predominant left hemisphere metabolic dysfunction in dementia. Arch. Neurol. 46 (2), 146–152.
Yang, C., Zhong, S., Zhou, X., Wei, L., Wang, L., Nie, S., 2017. The Abnormality of Topological Asymmetry between Hemispheric Brain White Matter Networks in Alzheimer's Disease and Mild Cognitive Impairment. Front. Aging Neurosci. 9, 261.
Walters, K.F., Shukla, R., Kumar, V., Schueren, S., Yadav, H., Schilaty, N.D., et al., 2025. Resting-State EEG Power Spectral Density Analysis between healthy and Cognitively Impaired Subjects. Brain Sci. 15 (2).
Wang, J., Fang, Y., Wang, X., Yang, H., Yu, X., Wang, H., 2017. Enhanced Gamma activity and Cross-Frequency Interaction of Resting-State Electroencephalographic Oscillations in patients with Alzheimer's Disease. Front. Aging Neurosci. 9, 243.